41st AIAA/ASME/SAE/ASEE Joint Propulsion Conference
Tucson, AZ, July 10-13, 2005

AIAA-2005-3887

Computational Modeling of a Miniature Ion Thruster Discharge

Richard Wirz*
Jet Propulsion Laboratory, California Institute of Technology, Pasadena, CA

In this study the Discharge Chamber Model (DCM) simulates a 3-cm diameter ring-cusp ion thruster to validate the model at miniature scales and reveal important aspects of small ion thruster performance and behavior. In general, DCM results agree well with miniature thruster data. Simulation of an early version of the Miniature Xenon Ion (MiXI) thruster show that over 50% of the primary electrons are lost to the anode before having a collision with a propellant atom, thus revealing poor primary electron utilization in comparison with conventional NSTAR-size thrusters. Combining this observation with the discharge stability concerns at higher magnetic fields demonstrates that magnetic field optimization for a miniature ion thruster is bracketed by considerations of primary electron utilization and discharge stability. DCM results also show that the ionization in the thruster is almost entirely due to the primary electrons and that the secondary electron population attains relatively meager temperatures of only ~2eV. Discharge plasma densities are near NSTAR values (~2e17 m^{-3}) while neutral atom densities are relatively high (~1e19 m^{-3}). The combination of these plasma parameters results in plasma characteristics (i.e., electron collision ratio and plasma magnetization) that are very similar to that of the NSTAR thruster. A design sensitivity analysis shows that DCM is sufficiently accurate to aid in the design and optimization of miniature thrusters.

Nomenclature

B = magnetic flux density

$D_{||}$ = parallel plasma diffusion coefficient

$D_{\perp}$ = perpendicular plasma diffusion coefficient

D_B = Bohm diffusion coefficient

f_{inel} = secondary inelastic collision fraction

f_A = fraction of ion current to anode surfaces

f_B = fraction of ion current to the beam

f_C = fraction of ion current to cathode surfaces

F_B = beam flatness

J_B = total beam current

J_B^+ = beam current due to singly charged ions

J_B^{++} = beam current due to doubly charged ions

J_D = discharge current

J_{DCH} = discharge cathode heater current

J_i = current of ions created in discharge

J_{ip} = current of ions created in discharge by primaries

J_p = primary electron current

J_{screen} = screen grid ion current

$\dot{m}_d$ = discharge chamber propellant mass flow rate

n_e = secondary electron number density

n_i = ion number density (total)

n_o = neutral atom number density

n_p = primary electron number density

$\dot{n}_e$ = secondary generation rate density

$\dot{n}_i$ = total ion generation rate density

(P_{ps}, P_{pw}, P_{piz}, P_{px}, P_{sw}, P_{siz}, P_{sx}) = electron power loss mechanisms (described in text)

r = distance from thruster axis

T_e = secondary electron temperature

T_i = ion temperature

T_p = primary electron temperature

T_o = neutral atom temperature

V_{accel} = accelerator grid voltage

V_B = beam voltage

V_D = discharge voltage

V_p = primary electron voltage

Greek Symbols

δ_D = plasma magnetization

δ_ν = electron collision ratio

ε_B = discharge loss

γ_{nc} = non-classical collision parameter

Γ = particle flux

Γ_e = electron flux

$\eta_{ud\,[Gas]}$ = discharge propellant utilization efficiency per Neutral Atom Sub-Model

©2005 by the American Institute of Aeronautics and Astronautics, Inc. The U.S. Government has a royalty-free license to exercise all rights under the copyright claimed herein for Governmental purposes. All other rights are reserved by the copyright owner.
*Staff Engineer, Advanced Propulsion Technology Group

$\eta_{ud\,[Beam]}$ = discharge propellant utilization efficiency per Ion Diffusion Sub-Model

η_{ud} = discharge propellant utilization efficiency

$\nu_{e\text{-}o}$ = neutral-centered electron collision frequency

$\nu_{e\text{-}i}$ = ion-centered electron collision frequency

ζ_o = grid transparency to neutral atoms

ζ_i = grid transparency to ions

Units:

This study uses mks units of the International System (SI) with the exception that energies are frequently given in terms of electron volts (eV).

sccm ≡ Standard Cubic Centimeters per Minute. For xenon: 1 sccm ≈ 0.09839 mg/s at STP.

eV/ion ≡ (Watts of Discharge Power)/(Amp of Beam Current) for discharge loss, ε_B

I. Introduction

A. Background and Motivation

The discharge performance of DC ring-cusp ion thrusters generally decreases for smaller discharge sizes. This trend is commonly attributed to higher wall losses associated with greater surface-to-volume ratio; however, previous studies have failed to identify the fundamental mechanisms associated with miniature discharges [1]. Experimental investigations of "Micro-Ion" and Miniature Xenon Ion (MiXI) thruster performance have shown that increasing the magnetic field strength in an effort to achieve greater plasma confinement leads to discharge instabilities [2-4]. Desirable performance for these thrusters has been demonstrated at low magnet weight and further improvement of the discharge performance is possible. Computational modeling of these discharges should help identify important plasma processes and aid in thruster optimization. The Discharge Chamber Model (DCM) has revealed important information on discharge processes for the NSTAR thruster and successfully predicted performance improving design modifications [5]. If validated at miniature thruster scales (~3cm diameter), DCM should yield similar benefits for the MiXI thruster design.

B. Objective

This study validates DCM at miniature ion thruster sizes by comparing with experimental data from the Micro-Ion thruster, which was developed at Caltech/JPL to guide the design of the patent-pending MiXI thruster. A combination of experiments, theory, and computational modeling from this and previous studies are used to identify the challenges of miniature discharge design. The results provide insight to the following questions about miniature DC ring-cusp ion thruster discharges:

1) What is the relative importance of the primary and secondary electron species?

2) How do the characteristics of miniature ion thruster discharges compare with conventional thruster discharges?

3) What are factors that lead to low performance for miniature ion thrusters?

II. General Approach

A. Discharge Chamber Model (DCM) Applied to Miniature Ion Thruster Discharges

This section contains a brief overview of the DCM computational model used in this study and focuses on some of the special considerations that are associated with modeling miniature discharges. For the interested reader, a more thorough overview of the model is in reference [5] while a detailed formulation is in reference [1].

The multi-component hybrid 2D computational discharge model, DCM, simulates ion thruster discharge processes and provides a framework for a full thruster model. The model is designed to integrate thruster component (cathode and grid) wear models to allow the determination of thruster life and long-term performance. DCM accounts for the five major chamber design parameters (chamber geometry, magnetic field, discharge cathode, propellant feed, and ion extraction grid characteristics) and self-consistently tracks four plasma species (neutral propellant atoms, secondary electrons, primary electrons, and ions).

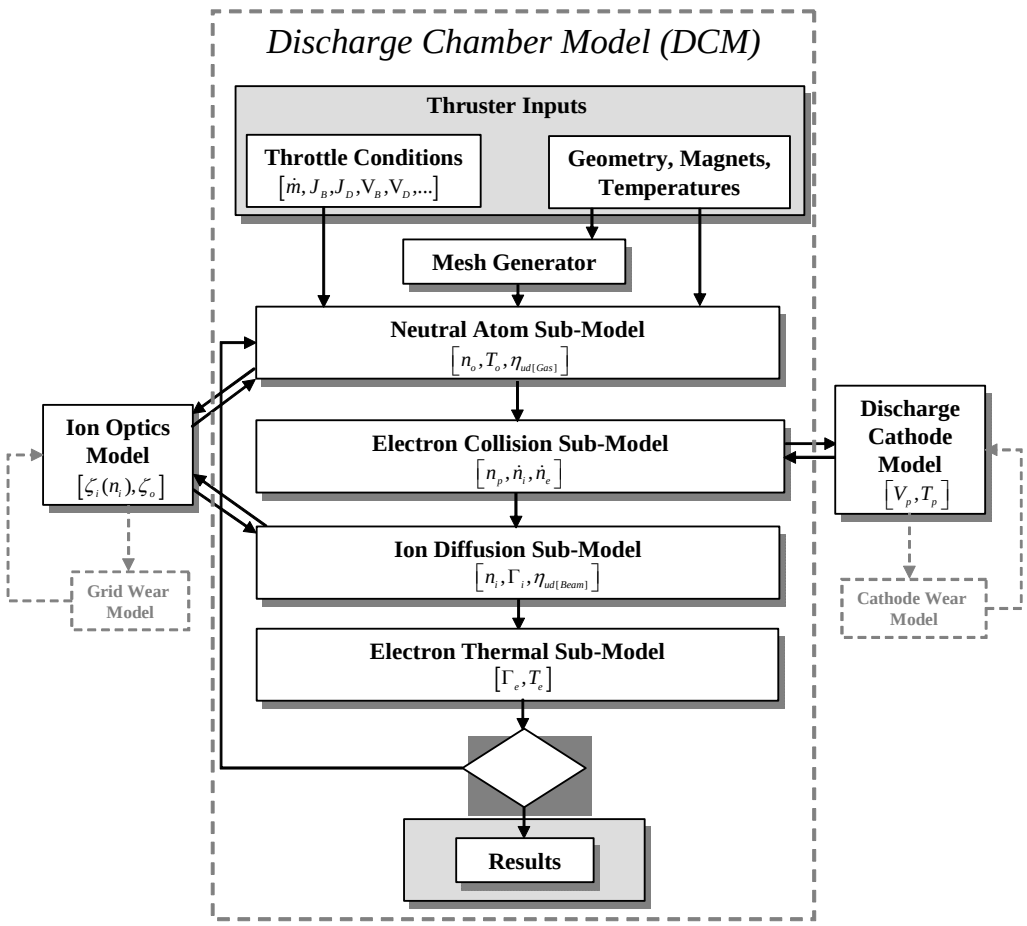

Figure 1. Discharge chamber model flowchart.

DCM is composed of the species-specific sub-models as shown in Figure 1. The sub-models use computational techniques that yield sufficient accuracy while minimizing run-time. For example, the 2D neutral atom sub-model is based on techniques used to calculate thermal transport view factors. This technique provides over an order of magnitude savings in run-time compared to a simple 2D steady-state Monte Carlo simulation used in preliminary versions of the code. In the Electron Collision Sub-Model, high-energy primary electrons are tracked with a Boris-type predictor-corrector algorithm. At this time, the primary electrons are assumed to populate an accelerated half-Maxwellian energy distribution that is

approximated from discharge cathode experimental data. The secondary electrons are treated as a quasi-neutral component of the plasma with a depleted-tail Maxwellian distribution. The Ion Optics Model determines grid transparency to ions and neutrals. Ion diffusion is assumed ambipolar and a non-classical correction is used for the perpendicular diffusion of secondary electrons. The Electron Thermal Sub-Model approximates the secondary electron distribution using detailed information of the transfer of primary electron energy to the secondary population. The model reaches a steady-state solution by first assuming very low density thermal plasma (at least an order of magnitude less than the anticipated final condition) and then incrementally increasing the primary electron current until full primary current is reached. Detailed descriptions of DCM assumptions and techniques are given in references [1] and [5].

For the magnetostatic field solution, DCM employs a simple corrected dipole solution technique. With this method the primary electron tracking algorithm calculates the magnetic field exactly at each point in its trajectory to avoid inaccuracies that can arise from magnetic field interpolation methods. This magnetostatic solution technique also results in faster run times and minimizes design modification effort in comparison to using external magnetostatic solution packages. The magnetostatic dipole solution is corrected in the dipole near-field (where the dipole solution is highly inaccurate) by assuming that the near-field magnetic contours are spherical and the magnetic field solutions on these spheres are equivalent to the analytical on-axis solutions for the permanent magnet [1]. This near-magnet correction of the dipole solution is important for smaller ion thruster discharges (i.e., 3cm diameter) where the inaccuracy of a simple magnetic dipole approximation would introduce magnetic field errors of well over 40% for more than half the chamber volume. It is also important at the magnetic cusps, where the artificially high near-magnet field strength predicted by a simple dipole approximation would greatly over predict primary electron confinement.

B. Miniature Ion Thruster Data

The experimental performance and beam profile data used in this study is from the "Micro-Ion" thruster [3], which was the test bed for designing the patent-pending Miniature Xenon Ion (MiXI) thruster [4].

III. Results

A. Inputs and Assumptions

The Micro-Ion thruster geometry simulated by the model is shown in Figure 2. All the propellant for the Micro-Ion thruster comes from a diffusion plate at the forward most surface of the chamber. Comparisons of the measured magnetic field and that predicted by the model, Figure 3, show some discrepancy, but the general shape and strength of the field is consistent.

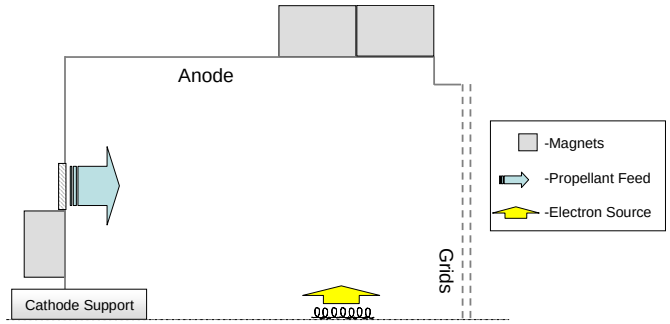

Figure 2. Micro-Ion Thruster 3-Ring Geometry used by DCM

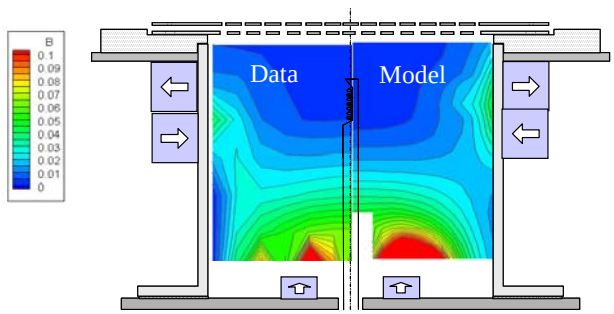

Figure 3. Comparison of magnetostatic |B| solution with Micro-Ion magnetic field contours (Tesla)

DCM simulated the Micro-Ion thruster operating conditions in Table 1, which is identified herein as throttle point "mTH1." The Ion Optics Model determines the ion and neutral transparencies using the grid voltages and grid geometry. The current of primaries from the cathode is determined from charge conservation by $J_p = J_D - J_{screen}$, where J_{screen} is the ion current to the screen grid determined by the Ion Diffusion Sub-Model. As discussed in reference [1], the primary electrons are assumed to possess a half-Maxwellian energy distribution for hollow cathode discharges, however, the electrons from the Micro-Ion thruster's filament discharge cathode are assumed to behave as single-energy primary electrons, implying $T_p \approx 0$eV. Using the voltages in Table 1 and assuming the plasma potential to be 2-3V, the initial guess for primary energy was $V_p \sim 22$V. Ultimately, a voltage of $V_p = 21$V yielded the beam current for mTH1, so this value was used for the results herein. Similarly to reference [5], the secondary inelastic collision factor, f_{inel}, is assumed equal to 0.8, and the non-classical diffusion parameter, γ_{nc} is ¼.

Table 1. Micro-Ion Throttle Point mTH1

Total Flow (sccm)	J_B (mA)	J_D (mA)	V_D (V)	V_B (V)	V_{accel} (V)	Model Specific Inputs	
						Vp (V)	Tp (eV)
0.29	14.05	293.5	25.0	911	-211	21	0

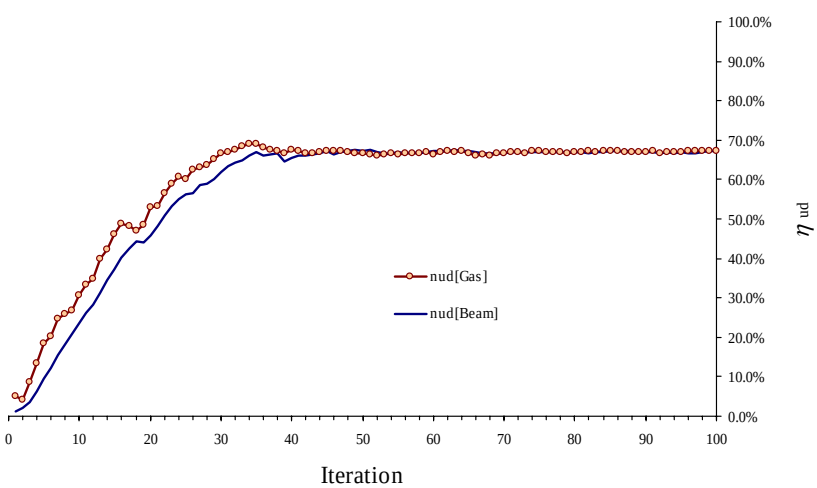

Figure 4. Propellant Efficiency vs. Iteration for mTH1

B. Model Results and Experimental Comparison

The results in this section are for DCM at mTH1, unless otherwise noted. The Micro-Ion simulations required relatively slow growth rates of the primary electron current, in comparison to NSTAR simulations [5], to avoid large gradients in the early iterations.

Solution Convergence

Figure 4 shows the results for propellant efficiency vs. iteration

where the primary current reached full strength after 30 iterations. In this figure, nud[Gas], nud[Beam] are the propellant efficiencies found by the Neutral Atom Sub-Model and Ion Diffusion Sub-Model as discussed in reference [5]. Since the single-energy primary electron value of 21V is below the double ionization threshold for xenon, double ion effects are not seen in these results. The presence of double ions is likely very small for the Micro-Ion thruster because $n_o >> n_i$, as determined by experimental measurements [3].

The convergence of the volume-averaged densities is shown in Figure 5. In comparison to NSTAR, the ion and primary densities are of the same order; however the neutral density is over an order of magnitude higher. Plots of these parameters on the Internal Mesh are given below.

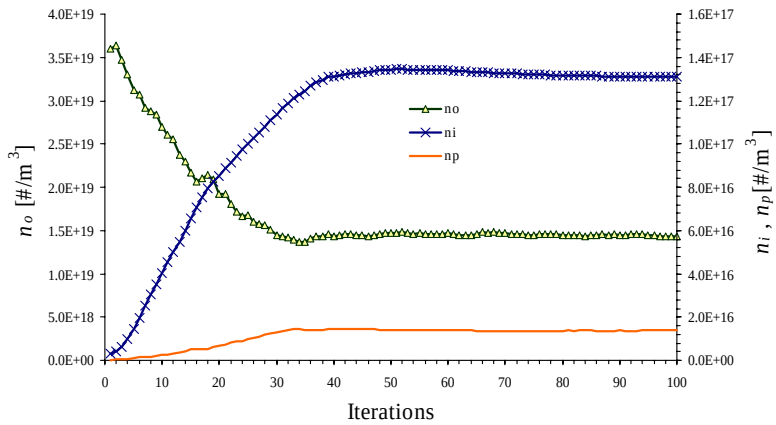

Figure 5. Volume-Averaged Densities vs. Iteration for mTH1

Comparison with Experimental Results

Beam current density profiles along the flat exit plane of the thruster are shown in Figure 6. The "Data" profile is the experimentally derived profile from reference [3] for operating point mTH1. The profile from DCM, jB[+], shows generally good agreement with the Data profile, except for the higher densities predicted near the center and the edge of the grids. The neutral atom profile is very flat, especially in comparison to the results for the NSTAR thruster [5].

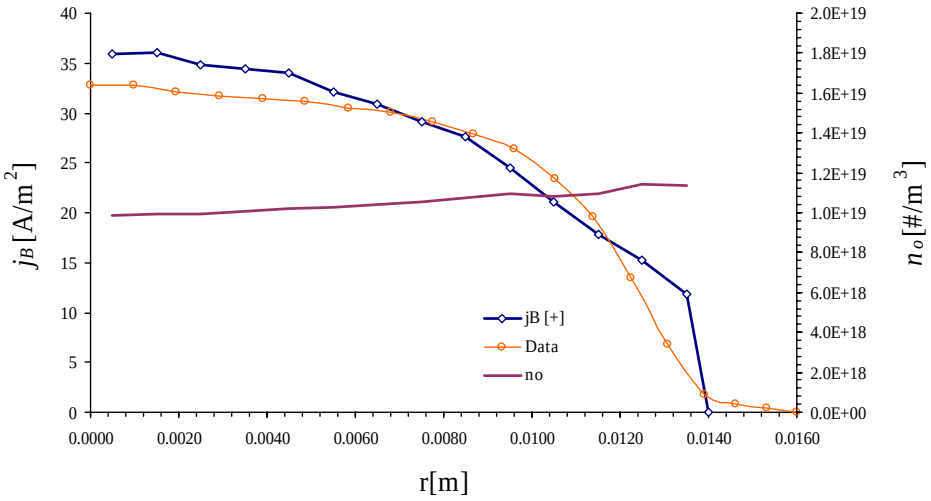

Figure 6. Beam and Neutral Density Profiles at Grids for mTH1

Discharge Performance Parameters

The results of the model are expressed by averaged discharge performance parameters at the Micro-Ion mTH1 operating condition and are compared to the thruster data in Table 2. Variable definitions are given in the nomenclature list. The agreement of η_{ud} and ε_B is a consequence of the choice of throttle point. Comparing J_i and J_{ip} shows that the primary electrons are responsible for ion generation in the Micro-Ion thruster.

Table 2. Discharge Performance Parameters for mTH1 (Micro-Ion Simulation vs. Data)

Discharge Parameters	η_{ud}	ε_B	J_{B++}/J_{B+}	J_i	J_{ip}	n_i	n_p	n_o	f_A	f_B	f_C	F_B
Units	%	eV/ion		mA	mA	m^{-3}	m^{-3}	m^{-3}	-	-	-	-
Model Results	67.1	520	0	56.8	56.5	$1.31 *10^{17}$	$1.39 *10^{16}$	$1.44 *10^{19}$	0.54	0.25	0.21	0.64
Data	66.9	522	-			$\sim 2.0 *10^{17}$						0.67

Electron Power Loss

Power loss parameters are defined below to compare the electron behavior in Micro-Ion and NSTAR discharge chambers. The *total* input energy is defined by the total primary current and the average primary energy. The secondary electron energy losses are referenced to the *total* input power to assess their contribution to the overall power balance of the discharge. Therefore, by the following definitions, $P_{ps} = P_{sw} + P_{siz} + P_{sx}$.

P_{ps} – primary power transferred to secondary population

P_{pw} – primary loss to wall

P_{piz} – primary ionization of propellant

P_{px} – primary excitation of propellant

P_{sw} – secondary loss to walls

P_{siz} – secondary ionization of propellant

P_{sx} – secondary excitation of propellant

The results in Table 3 show that the primary electrons are more likely lost to the wall before imparting energy to other plasma species, which results in relatively high discharge loss for mTH1.

Table 3. Electron Power Loss Mechanisms (Micro-Ion vs. NSTAR)

Mechanism	**Primary Electron Losses**				**Secondary Electron Losses**		
	P_{ps}	P_{pw}	P_{piz}	P_{px}	P_{sw}	P_{siz}	P_{sx}
Micro-Ion (mTH1)	20.9%	58.2%	12.1%	8.8%	20.6%	0.1%	0.2%
NSTAR (TH15)*	69.0%	0.7%	13.7%	16.6%	49.1%	7.5%	12.5%

*Reference 5

Two-Dimensional Plots of Discharge Characteristics

In the following figures generated by DCM, the non-uniform behavior of the Micro-Ion thruster at mTH1 is summarized with plots of ion and neutral density, and ion generation rate. The total ion density distribution, Figure 7, is peaked near the cathode but relatively flat across the grid plane. The neutral density profile shown in Figure 8 is essentially uniform and reveals that n_o is almost two orders of magnitude greater than n_i throughout the chamber. Figure 9 shows the distributed ion generation rate, which is almost entirely due to primary electron ionization since $J_{ip}/J_i \sim 1$. For the nearly uniform neutral density, this ionization profile mimics the primary electron density profile. A plot of five example primary

electron paths, Figure 10, shows that the 3-Ring configuration confines the primary electrons near the grids, resulting in a relatively high ionization rate in that region. The secondary electron temperature, not shown, was essentially uniform at $T_e \sim 2$ eV for the Micro-Ion thruster simulations herein. At this meager temperature, the secondaries do not provide appreciable ionization.

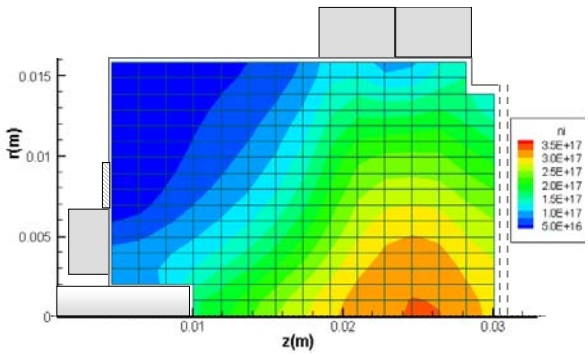

Figure 7. Total (Single) Ion Density (m^{-3}) - mTH1

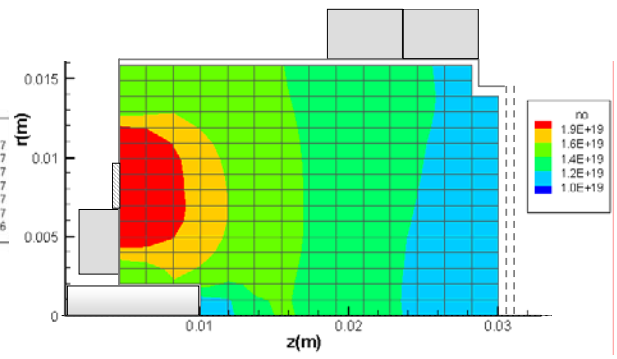

Figure 8. Neutral Atom Density (m^{-3}) – mTH1

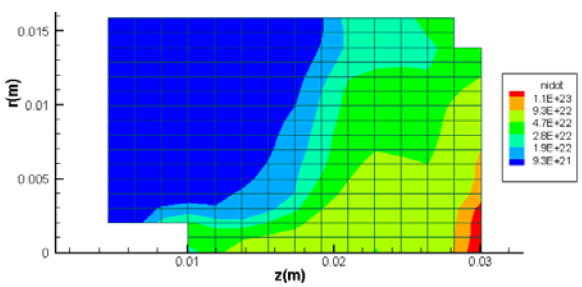

Figure 9. Ion Generation Rate Density ($s^{-1}m^{-3}$) - mTH1

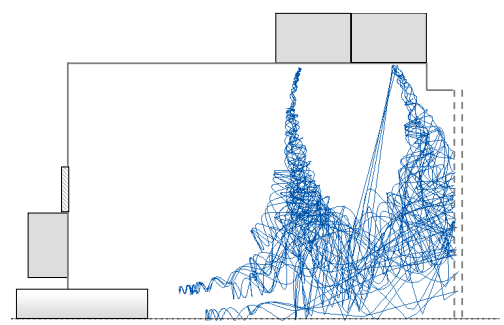

Figure 10. Example Primary Electron Paths

The electron collision ratio, δ_ν (the ratio of electron-neutral-centered and electron-ion-centered collisions, $\delta_\nu \equiv \nu_{e\text{-}o}/\nu_{e\text{-}i}$), distribution plotted in Figure 11 shows that even in the presence of a relatively high neutral density, the plasma is intermediately ionized throughout the chamber and increasingly ionized on-axis. In this intermediately ionized regime, the plasma magnetization δ_D, is similar to that of the NSTAR thruster [5]. Details of the parameters δ_ν and δ_D are given in references [1] and [5].

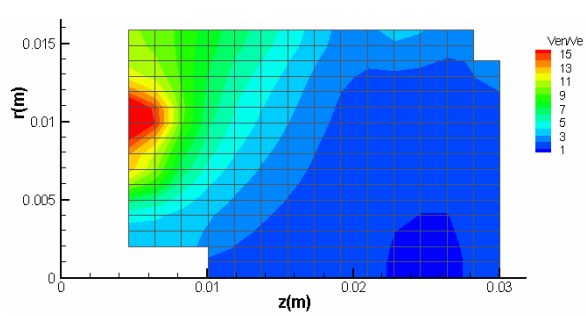

Figure 11. Electron Collision Ratio ($\delta_\nu = \nu_{e\text{-}o}/\nu_{e\text{-}i}$) - mTH1

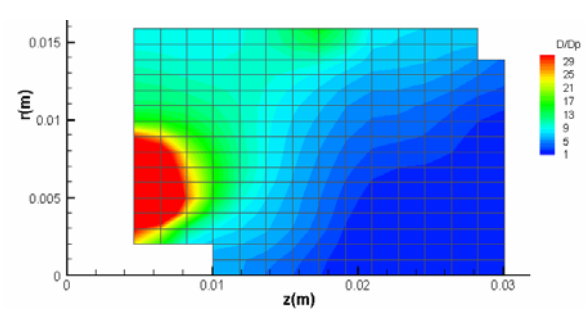

Figure 12. Magnetization, Plasma Diffusion Coefficient Ratio ($\delta_D = D_{||}/D_\perp$) - mTH1

C. Miniature Thruster Design Analysis

An experimental sensitivity analysis of the axial location of the mid magnet ring of the original Micro-Ion thruster configuration was conducted by spacing the anode magnet rings as shown in Figure 13. The results of these tests suggests that the discharge loss, ε_B, decreases noticeably if the mid magnet ring is spaced less than 2mm from the grid magnet ring. Referring to Figure 13, the model predicts the performance trend due to magnet spacing; however, the reduction in discharge loss is not as drastic as found in the experimental results. The impact of this modification on the discharge parameters is shown in Table 4 by comparing the discharge performance parameters with the original thruster design.

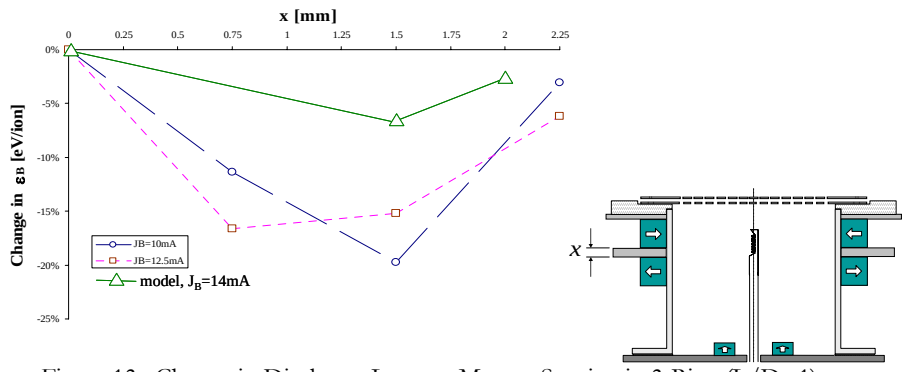

Figure 13. Change in Discharge Loss vs. Magnet Spacing in 3-Ring (L/D=1) Configuration of Micro-Ion Thruster, Compared with Discharge Model Result

Table 4. Discharge Performance Parameters at mTH1 (Micro-Ion Original vs. Modified Design)

Discharge Parameters	η_{ud}	ε_B	J_{B++}/J_{B+}	J_i	J_{ip}	n_i	n_p	n_o	f_A	f_B	f_C	F_B
Units	%	eV/ion	-	mA	mA	m^{-3}	m^{-3}	m^{-3}	-	-	-	-
Original	67.1	520	0	57.4	57.1	$1.31 *10^{17}$	$1.39 *10^{16}$	$1.44 *10^{19}$	0.66	0.29	0.05	0.64
Modified (1.5mm magnet spacing)	67.7	490	0	61.9	61.6	$1.5 *10^{17}$	$1.62 *10^{16}$	$1.40 *10^{19}$	0.56	0.23	0.21	0.57

The profiles for the modified design, Figure 14, show the more peaked profile in comparison to the experimental "Data" for the original configuration. Therefore, though many of the discharge parameters in Table 2 are favorable for the modified design, the profile data (and resulting F_B) suggest that this design may not be preferable if the non-uniformity of the beam leads to undesirable grid life.

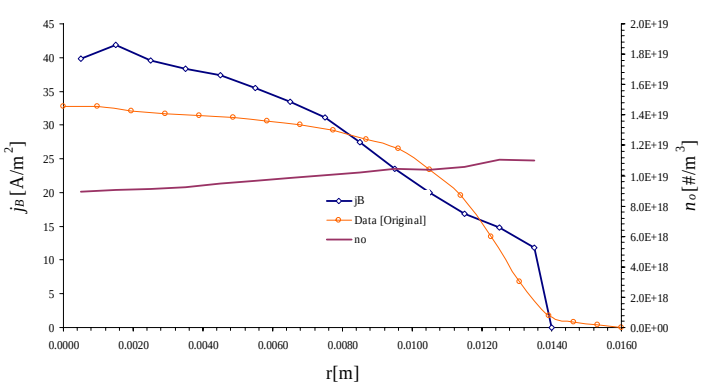

Figure 14. Beam and Neutral Density Profiles for the Modified Micro-Ion Thruster - mTH1 (note: "Data" values are from original thruster configuration)

VI. Conclusions

DCM results for the Micro-Ion thruster show that the discharge ionization is almost entirely due to primary electrons and approximately half of the primaries are lost to the walls before having an inelastic collision. The high wall losses for the miniature chamber yield meager secondary temperatures of only about 2eV, resulting in negligible secondary ionization. The low ionization efficiency of the miniature discharge requires proportionally high propellant flow rates, and hence densities, to attain ion densities similar to those found in the NSTAR thruster. This results in neutral densities nearly two orders of magnitude greater than ion density throughout the discharge chamber. Nonetheless, the electron collision ratio, δ_ν, was found to be sufficiently low such that the miniature discharge plasma diffusion is in a similar regime to that of the NSTAR discharge. This result can be explained by the sharp drop-off of the total electron-neutral collision cross-section for xenon at $T_e \approx 2$eV. The low electron collision ratio, δ_ν, in the Micro-Ion discharge results in low levels of plasma magnetization, δ_D.

Recognizing the poor primary confinement of the Micro-Ion discharge leads to the consideration of higher magnetic fields to better confine the primaries. However, higher magnetic fields resulted in poor performance for the 3-ring configuration. This poor performance can be explained by the onset of discharge instabilities due to overly high cusp magnetic field strengths [3]. In this way, miniature ion thruster discharges demand careful consideration of the competing effects of efficiency and stability. The larger surface-to-volume ratio requires high cusp B-field strength for favorable primary utilization; while the cusp B-field strength for a given magnetic field geometry must be sufficiently low to assure discharge stability through the desired range of operating conditions. These observations suggest that miniature ion thruster performance is bracketed by primary electron utilization and discharge stability.

The experimental efforts outlined in reference [1] were able to identify a relatively efficient miniature discharge configuration; however, additional optimization of the precise magnetic field strength and placement should lead to noticeable improvements in discharge performance. In its present form, the model can be used to determine thruster designs that yield improved primary electron confinement, while experimental testing can be used to assess the stability of these designs. The performance degradation due to high magnetic field strengths (i.e., discharge stability) needs to be characterized and incorporated into future versions of DCM.

Acknowledgments

The research described in this paper was carried out by the Jet Propulsion Laboratory, California Institute of Technology, under a contract with the National Aeronautics and Space Administration in support of Project Prometheus.

References

[1] – Wirz R., "Discharge Plasma Processes of Ring-Cusp Ion Thrusters," Ph.D. Dissertation, Aeronautics, Caltech, Pasadena, CA, 2005

[2] – Wirz R., Polk J., Marrese C., Mueller J., "Development and Testing of a 3cm Electron Bombardment Micro-Ion Thruster," IEPC Paper 01-343, 27th IEPC, Pasadena, CA, Oct 2001

[3] – Wirz R., Polk J., Marrese C., Mueller J., "Experimental and Computational Investigation of the Performance of a Micro-Ion Thruster," AIAA-2002-3835, 38th JPC, Indianapolis, IN, July 2002

[4] – Wirz R., Mueller J., Gale M., Marrese C., "Miniature Ion Engine for Precision Formation Flying," AIAA-2004-4115, 40th Joint Propulsion Conference, Ft. Lauderdale, FL, 2004

[5] – Wirz R., Katz I., "Plasma Processes of DC Ion Thruster Discharge Chambers," AIAA Paper 2005-3690, 41st AIAA Joint Propulsion Conference, Tucson, AZ, 2005.